Organic Electronics 17 (2015) 295–303

Contents lists available at ScienceDirect

Organic Electronics

journal homepage: www.elsevier.com/locate/orgel

Toward efficient non-fullerene polymer solar cells: Selection of donor polymers

Long Ye [a,c], Wei Jiang [b], Wenchao Zhao [a], Shaoqing Zhang [a], Yong Cui [a], Zhaohui Wang [b,*], Jianhui Hou [a,*]

[a] State Key Laboratory of Polymer Physics and Chemistry, Beijing National Laboratory for Molecular Sciences, Institute of Chemistry, Chinese Academy of Sciences, Beijing 100190, PR China

[b] CAS Key Laboratory of Organic Solids, Beijing National Laboratory for Molecular Sciences, Institute of Chemistry, Chinese Academy of Sciences, Beijing 100190, PR China

[c] University of Chinese Academy of Sciences, Beijing 100049, PR China

ARTICLE INFO

Article history:
Received 10 October 2014
Received in revised form 11 December 2014
Accepted 13 December 2014
Available online 24 December 2014

Keywords:
Polymer solar cells
Perylene bisimides
Non-fullerene acceptor
Donor polymers

ABSTRACT

Recently, perylene bisimides have been explored and developed as potential candidates for non-fullerene acceptors and power conversion efficiencies (*PCE*s) exceeding 3% were realized in the non-fullerene polymer solar cells (NF-PSCs) featuring perylene bisimides as acceptors. Considering that only a few donor polymers like P3HT and PBDTTT-C-T were utilized in non-fullerene PSCs, screening donor polymers with well-matched energy levels, absorption spectrum as well as hole mobility in NF-PSCs will be the key to promote the current *PCE*s. Herein, four high performance donor polymers including PBDTTPD, PBDTTT-EFT, PDPP3T, PSBTBT were employed for the optimization of single bond-linked perylene bisimide (SDIPBI)-based NF-PSCs. A clear criterion in selection of donor polymers has been established for the SDIPBI-based NF-PSCs. Suitable energy level differences, finer morphology, and broad absorption ranges could be successively screened for donor polymers. Interestingly, NF-PSCs based on PBDTTPD/SDIPBI delivers a high V_{oc} of 1.04 V and a desirable PCE of 3.4%. Moreover, the SDIPBI-based NF-PSC employing PBDTTT-EFT as donor polymer exhibits a high PCE up to 4.5%. The results implicate that to select donor polymers is a feasible strategy to boost the photovoltaic performance of NF-PSCs further.

1. Introduction

Polymer solar cells (PSCs), made by solution processed organic/polymeric photoactive materials have shown great promise as a disruptive technology for affordable electricity [1–6]. Typically, polymers act as donor materials and organic molecules like fullerene derivatives served as acceptor materials in the photoactive layers of PSCs. Fullerene derivatives such as [6,6]-phenyl-C_{61}(or C_{71})-butyric acid methyl ester (PCBM) have become the predominantly used acceptor materials in PSCs since the pioneer work of Wudl, Heeger and co-workers in 1995 [7]. To address the problems like weak absorption and high-cost production in PCBM, various efficient non-fullerene small molecules have been explored as alternatives to PCBM in PSCs over the past three years and delivered power conversion efficiencies (*PCE*s) over 3% [8,9]. Relative to the high *PCE*s exceeding 8.5% in polymer/PCBM solar cells [10–27], increased efforts to develop highly efficient non-fullerene polymer solar cells (NF-PSCs) are still needed due to the relatively low *PCE* values. Actually, a majority of non-fullerene small molecule acceptors are routinely blending

* Corresponding authors. Tel.: +86 10 82615900.
E-mail addresses: zhaohuiwang@iccas.ac.cn (Z. Wang), hjhzlz@iccas.ac.cn (J. Hou).

http://dx.doi.org/10.1016/j.orgel.2014.12.020
1566-1199/

with poly(3-hexylthiophene) (P3HT), which is not the best choice of donor polymer in NF-PSCs [28–32]. Considering P3HT possesses an absorption edge of 650 nm and a high-lying highest occupied molecular orbital (HOMO) level of −4.9 eV [1], the device characterization merely utilizing P3HT might miss some excellent non-fullerene acceptors due to the relatively narrow spectral coverage and the mismatch between the energy levels of P3HT and the acceptors.

Recent investigations revealed that rationally screening novel donor polymers is an effective approach for meliorating the low photovoltaic performance of NF-PSCs, especially for perylene bisimides (PBI) dimmers systems [33–44]. We also noted that PBI-based monomers and polymers [35–39] are also successfully applied in PSCs as fullerene-free acceptors. Compared with PBI-based monomers and polymers, PBI dimers exhibited non-planer structures to reduce intermolecular interactions and thus molecular aggregations. For instance, Narayan and co-workers firstly introduced a low band gap polymer PBDTTT-C-T into a twisted PBI dimer-based NF-PSC and obtained a considerable *PCE* up to 3.20% [40,41]. Other groups and we also found that PBDTTT-C-T exhibited wide applicability with a range of non-fullerene small molecule acceptors and produced several impressive advances in NF-PSCs [40–47]. In our previous work, by replacing PBDTTT-C-T with a wide band gap polymer PBDTBDD as donor material, the *PCE* of singly-linked perylene bisimides (SDIPBI)-based PNFSCs were promoted to 4.39% [46]. Very recently, Jen, Wang and co-workers [47] applied a superior low band gap polymer into SDIPBI-based PSC also boosted the *PCE* up to 4.21%. Moreover, they further achieved a superior *PCE* with inverted device structure and broke 5% barrier in NF-PSCs. Clearly, these works firmly emphasized the beneficial effects of choice of novel donor polymers in NF-PSCs.

Inspired by the versatility and excellence of SDIPBI in NF-PSCs, novel photovoltaic polymers with different energy levels and absorption spectra as donor polymers might be the key to promote the current *PCE*s. In the present work, we focus on SDIPBI-based NF-PSCs by comprising some of the efficient and well-known photovoltaic polymers including PBDTTPD [48], PBDTTT-EFT [23–26], PSBTBT [49], PDPP3T [50,51] as donor materials (Fig. 1) and also refine the selection rules of donor polymers in NF-PSCs. Interestingly, the PBDTTPD/SDIPBI-based NF-PSCs delivers a high open-circuit voltage (V_{oc}) of 1.04 V along with a high *PCE* of 3.4%. Moreover, the PBDTTT-EFT/SDIPBI-based NF-PSC realizes a high short-circuit current density (J_{sc}) of 11.5 mA/cm^2 and an outstanding *PCE* of 4.48%.

2. Experimental section

2.1. Materials

SDIPBI was synthesized using the identical procedure as our previous report [46]. The four donor polymers (PBDTTPD [48], PBDTTT-EFT [23–26], PSBTBT [49], and PDPP3T [50,51]) were synthesized in our laboratory according to the previous literatures. The number-average molecular weights (M_n) and polydispersities (PDI) of these donor polymers measured by high temperature GPC were provided in Fig. S1 and Table S1, see Supporting information for details. The processing solvents used in device fabrication process were purchased from Alfa Aesar. The PEDOT:PSS (Heraeus Clevios™ P VP AI 4083) and metal materials are commercial available products.

2.2. Fabrication and Characterization of PSC devices

Devices of polymer: SDIPBI blends (2:1, 1: 1 or 1:2 by weight) were fabricated using the same method as our previous report [45] with a conventional ITO/PEDOT:PSS (~35 nm)/active layer/Ca (20 nm)/Al (100 nm) structure. A polymer concentration of 10 mg/ml in chlorobenzene was adopted. Small amount of 1,8-diiodooctane and 1-chloronaphthalene were used as binary solvent additives, according to the previous report [46]. The active layer thickness was ∼90 nm as measured by a Bruker Dektak XT profilometer. Five pixels, each with an active area of ~0.04 cm^2 were fabricated per ITO substrate (1.5 cm × 1.5 cm). The current density–voltage (*J–V*) characteristics were measured under a Keithley 2400 Source Measure Unit under AM 1.5G 100 mW/cm^2 by the AAA grade XES-70S1 solar simulator (SAN-EI Electric Co., Ltd.). The space-charge-limited current (SCLC) current–voltage characteristics of the hole-only diodes were measure in the dark ambient conditions. Except for the deposition of the PEDOT:PSS layers, all the fabrication processes were carried out in a nitrogen glovebox containing less than 1 ppm O_2 and H_2O. The *EQE* curves were measured by the use of the Solar Cell Spectral Response Measurement System (QE-R3011, Enli Technology Ltd., Taiwan), and the light intensity at each wavelength was calibrated with a standard single crystal silicon photovoltaic cell. Absorption spectra were taken on a Shanghai Lab-spectrum 1900PC UV–Vis spectrophotometer, and XRD patterns of the blend films were measured using a Rigaku D/MAX 2500 X-ray diffractometer with a scan range of 3–30° . AFM measurements were performed using a MultiMode 8 Atomic Force Microscope (Bruker Inc.) in tapping mode. TEM images were obtained using a JEOL Transmission Electron Microscope (JEM-2200FS) with an accelerating voltage of 160 kV. TEM samples were prepared from actual devices that were transferred to an aqueous water solution, and then the floated photoactive films were then transferred to the commercial available copper grids. The electrochemical cyclic voltammetry (CV) was conducted on a Chi650D instrument with glassy carbon disk, Pt wire, and Ag/Ag$^+$ electrode as the working electrode, counter electrode, and reference electrode, respectively in a 0.1 M tetrabutylammonium hexafluorophosphate (n-Bu_4NPF_6)-anhydrous acetonitrile solution at a potential scan rate of 50 mV/s. Polymer film was drop cast onto the glassy carbon working electrode from a 2.0 mg/mL chloroform solution and dried under nitrogen stream prior to measurements. The electrochemical onsets were determined at the position where the current starts to differ from the baseline. The potential of Ag/Ag$^+$ reference electrode was internally calibrated by using the ferrocene/ferrocenium redox couple (Fc/Fc^+). Then, the energy levels were estimated using the following equations: $\mathrm{HOMO} = -(4.80 + E_{onset,\ ox})$, and $\mathrm{LUMO} = -(4.80 + E_{onset,\ red})$.

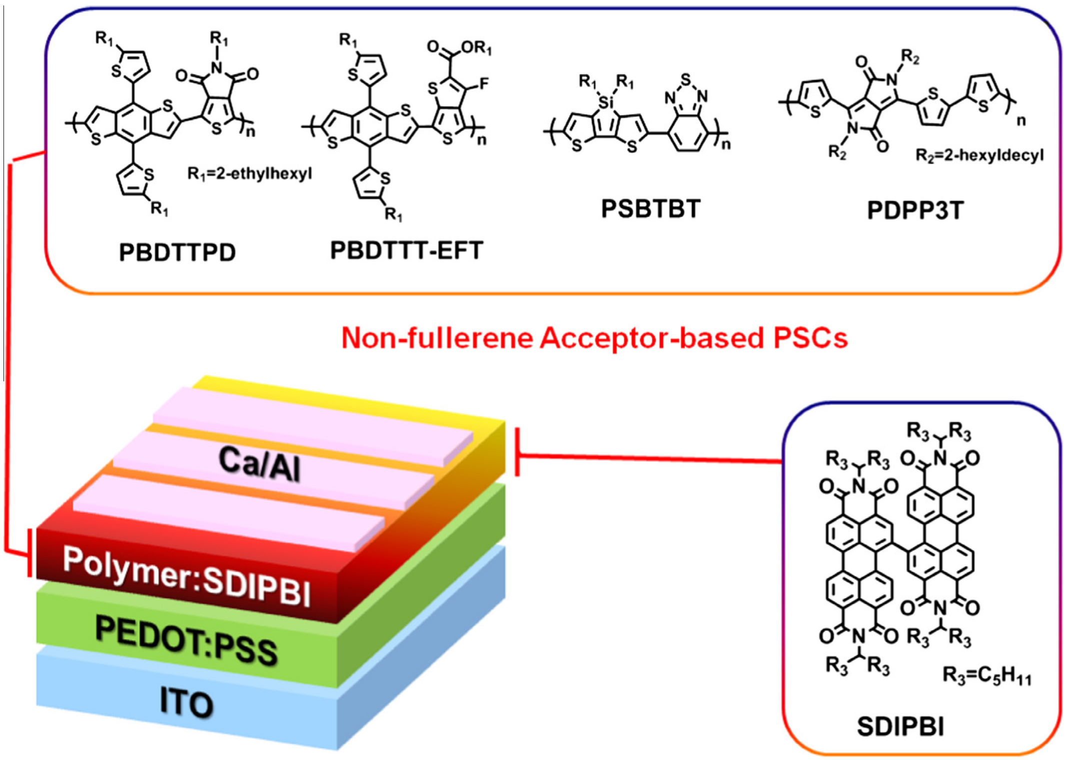

Fig. 1. The device diagram of NF-PSCs based on the involved donor polymers (PBDTTPD, PBDTTT-EFT, PSBTBT, PDPP3T) and non-fullerene small molecule (SDIPBI).

3. Results and discussion

3.1. Pristine properties of different donor polymers

In our previous work, a broad band gap polymer PBDTBDD was applied as donor polymer in SDIPBI-based NF-PSC [46]. As can be seen in Fig. 2a, the maximum absorption wavelength of PBDTBDD is limited at 700 nm and thus photons in the range of 700–900 nm could not be harvested. Considering only a few donor polymers like P3HT, PBDTBDD were utilized in NF-PSCs, some of the state-of-the-art photovoltaic polymers are respectively introduced to take the place of PBDTBDD in SDIPBI-based PSCs. Accordingly, the UV–vis absorption spectra of photovoltaic polymers are characterized with reference to the previously published PBDTBDD. As shown in Fig. 2b and Table 1, the absorption edge of PBDTTPD locates at ca. 680 nm, while other polymers all exhibit broader absorption ranges with absorption edges over 800 nm. PDPP3T gives a complementary absorption with SDIPBI, which covers the visible and near-IR regions. Thus, compared to the PBDTBDD-based NF-PSCs, improved short-circuit current

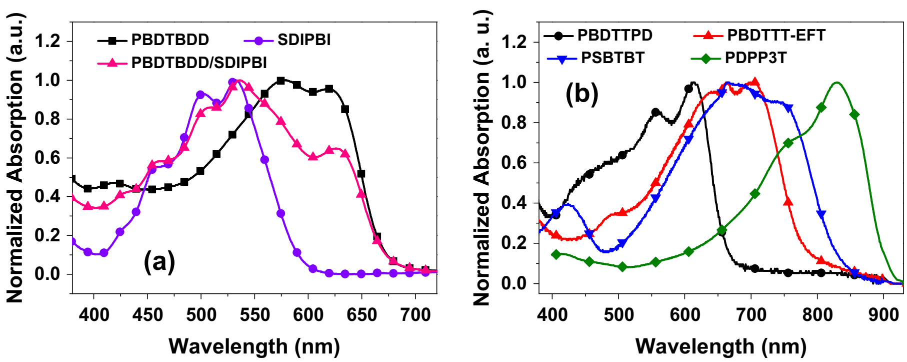

Fig. 2. (a) Absorption spectra of PBDTBDD, SDIPBI and PBDTBDD/SDIPBI blend film; (b) absorption spectra of the solid films of PBDTTPD, PBDTTT-EFT, PSBTBT and PDPP3T.

Table 1
Properties of the selected donor polymers and SDIPBI.

Materials	E_g^{opt} (eV)	λ_{edge} (nm)	HOMO level (eV)	LUMO level (eV)	Mobility[a] ($cm^2/(Vs)$)
PBDTTPD	1.82	680	−5.52	−3.24	4.7×10^{-4}
PBDTTT-EFT	1.58	785	−5.21	−3.48	4.4×10^{-3}
PSBTBT	1.45	855	−5.07	−3.17	5.1×10^{-4}
PDPP3T	1.33	932	−5.17	−3.28	8.5×10^{-3}
SDIPBI	2.08	608	−5.95	−3.87	2.0×10^{-4}

[a] Beside SDIPBI, all of the values represent the hole mobility.

densities could be expected in the NF-PSCs based on the low band gap polymers due to their broader absorption spectra.

Hole mobility is an important figure of merit to evaluate the charge transport properties of donor polymers. Estimated from the space charge limited current (SCLC) model (see Fig. S2), the hole mobilities of PBDTTPD, PBDTTT-EFT, PSBTBT, and PDPP3T are 4.7×10^{-4}, 4.4×10^{-3}, 5.1×10^{-4}, and 8.5×10^{-3} $cm^2\ V^{-1}\ s^{-1}$, respectively. All of these efficient donor polymers exhibit high hole mobility around the magnitude of 10^{-3} $cm^2/(V\ s)$, which is close to the electron mobility of SDIPBI ($\sim 10^{-4}$ $cm^2\ V^{-1}\ s^{-1}$) [46]. Accordingly, the mobility of the donor polymers would not necessary limit the charge transport properties in NF-PSCs.

Another important issue in NF-PSCs should be the match of energy levels of donor and acceptor materials [8]. In order to avoid getting misleading information, cyclic voltammetry of the four donor polymers in thin films is carried out to estimate their HOMO and LUMO in parallel, as shown in Fig. S3. The HOMO and LUMO levels estimated from the onsets of the oxidation and reduction processes are listed in Table 1 and the energy levels of SDIPBI are also listed for comparisons. As known, the V_{oc} of a bulk-heterojunction PSC is directly proportional to the gap between the LUMO of the acceptor material and the HOMO level of the donor material. Considering that SDIPBI exhibits a lowest unoccupied molecular orbital (LUMO) level of −3.87 eV [46], from the HOMO levels in Table 1, we could expect the PBDTTPD/SDIPBI blend should deliver a higher voltage output, while the PSBTBT/SDIPBI blend might exhibit a lower V_{oc}. According to previous evaluations of absorption spectra, molecular energy levels and hole mobility, these polymers might be potential candidates as the donor materials in SDIPBI-based PSCs.

3.2. Photovoltaic performances of the different donor polymers-based NF-PSCs

PSCs based on the aforementioned donor polymers with SDIPBI are fabricated using the conventional device architecture, as shown in Fig. 1. The D/A blend ratio optimizations are performed for different polymer/SDIPBI blends (see Table S2). Beside of PDPP3T, other polymers all deliver an optimal donor/acceptor blend composition of 1:1. Throughout the experiment, chlorobenzene (CB) is chosen as the host solvent and 1,8-diiodooctane (DIO)/1-chloronaphthalene (CN) is used as binary solvent additive to finely-manipulate the nano-morphologies of the blends, which has been verified in our previous works [46,47]. Fig. 3a presents the *J–V* curves under the optimized conditions. The corresponding performance parameters are tabulated in Table 2. The PDPP3T/SDIPBI-based PSC shows the lowest *PCE* (<1%) due to its low J_{sc} of ~3 mA/cm^2 and poor fill factor (*FF*) of ~38%. Similarly, the low band gap polymer PSBTBT blending with SDIPBI also exhibits a low *PCE* of ~1.7%. Remarkably, the PBDTTPD/SDIPBI-based NF-PSC delivers a high V_{oc} of 1.04 V along with a high *PCE* of ~3.4%. Although the V_{oc} is moderate (0.77 V), the NF-PSC composed of PBDTTT-EFT and SDIPBI gives an impressive performance, i.e. a J_{sc} of 11.5 mA/cm^2, a *FF* of 50.6% and thereby a *PCE* up to ~4.5%, which is a high value among NF-PSCs. Among these devices, the PDPP3T-based NF-PSCs provided an unexpected low J_{sc} value. This could be mainly attributed to the poor miscibility between PDPP3T and SDIPBI.

As depicted in Fig. 3b, the calculated J_{sc} values integrated from the *EQE* curves are quite consistent with the J_{sc} values obtained from the *J–V* measurements. The PBDTTPD/SDIPBI-based device exhibits high *EQE* values in the range of 350–650 nm with a peak value of 60% and the PBDTTT-EFT/SDIPBI-based device also depicts relatively high and broad quantum efficiency throughout the 450–750 nm wavelength range with a peak value of 55%. However, the quantum efficiency of the low band gap polymers, PSBTBT and PDPP3T, perform rather poor than that of PBDTTPD and PBDTTT-EFT. The PSBTBT-based device exhibits moderate *EQE* values of ~30% in the whole range of 400–800 nm. Although the response range of the PDPP3T/SDIPBI-based NF-PSC covers the whole visible range from 300 to 900 nm, the overall integral current density is very low due to the low *EQE* values, i.e. ~10% in the whole response range.

To probe the underlying device physical process such as exciton generation and dissociation, the photocurrent behaviors of the NF-PSCs based on different polymer/SDIPBI blends are characterized by sweeping the *J–V* curves from −5 to +3 V with a voltage step of 0.01 V [46,52]. The photocurrent density (J_{ph}) is given by $J_{ph} = J_L - J_D$, where J_L and J_D respectively represent the light and dark current density. The effective voltage (V_{eff}) across the device is given by the difference of compensation voltage (V_0, determined when the J_{ph} is zero) and applied voltage (V), and the saturation value of J_{ph} in the high V_{eff} region is defined as the saturation photocurrent density (J_{sat}). As depicted in Fig. 3c, J_{ph} is ploted against V_{eff} for each NF-PSC and the corresponding exciton dissociation probability ($P_{diss,}$ defined as the ratio of J_{ph} to J_{sat}) can be determined for these different polymer/SDIPBI blends under short circuit condition. A highest P_{diss} of 88.5% is achieved in the PBDTTT-EFT/SDIPBI-based device, while other

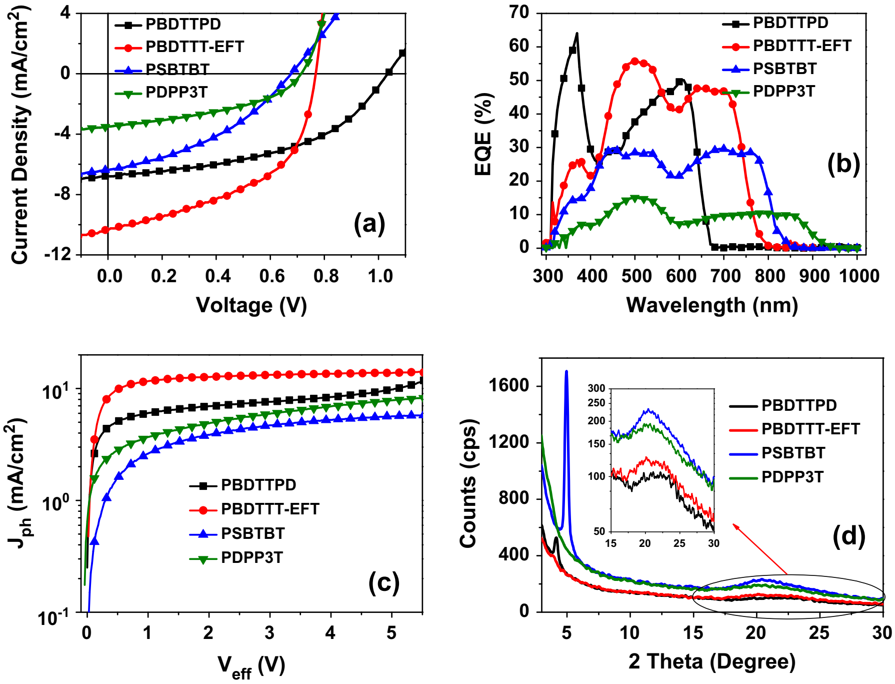

Fig. 3. (a) *J–V* curves, (b) *EQE* curves, (c) photocurrent behavior of polymer: SDIPBI blend films; (d) XRD spectra of polymer: SDIPBI blend films.

Table 2
Photovoltaic results of the SDIPBI-based NF-PSCs employing different donor polymers.

Donor polymer	V_{oc} (V)	J_{sc} (mA/cm^2)	*FF* (%)	PCE[a] (%)	P_{diss} (%)	R_q (nm)
PBDTTPD	1.04 ± 0.01	6.8 ± 0.2	47.6 ± 1.6	3.37 (3.27)	60.7	3.31
PBDTTT-EFT	0.77 ± 0.01	11.5 ± 0.2	50.6 ± 1.4	4.48 (4.39)	88.5	1.70
PSBTBT	0.68 ± 0.01	6.4 ± 0.2	38.4 ± 2.2	1.67 (1.55)	69.2	5.95
PDPP3T	0.71 ± 0.01	3.5 ± 0.3	40.3 ± 1.9	0.98 (0.84)	48.3	4.20

[a] The best values of photovoltaic parameters are obtained from 8 devices and the average PCE are listed in the parentheses.

polymer/SDIPBI blends possess rather poor P_{diss} (<70%), which could account for the relatively low J_{sc} in the corresponding devices. The high P_{diss} in PBDTTT-EFT/SDIPBI-based NF-PSC is comparable to the levels (80–90%) in the optimized fullerene-based PSCs [52], indicating that the photogenerated exciton dissociation could be also efficient in the fullerene-free systems. Particularly, a lowest P_{diss} of 48.3% is recorded for the PDPP3T/SDIPBI-based device.

3.3. Morphological properties of different donor polymer/SDIPBI blends

Since the molecule planarity of SDIPBI is weakened heavily by the twisted single bond linker, the crystallinity of SDIPBI is very weak in neat film (Fig. S4). Fig. 3d shows the microstructural information of different polymer/SDIPBI blend films investigated by X-ray diffractions (XRD), and it is worth noting that all of the polymer/SDIPBI blends yield some degree of π–π stacking feature, independent of the choice of donor polymers. The PBDTTPD/SDIPBI and PSBTBT/SDIPBI blends even exhibit apparent lamellar packing peaks. The different degree of crystallinity of polymer donors can manipulate the extent of polymer crystallization during the process of film formation and lead to distinct morphological features in these polymer/SDIPBI films. Generally, high crystallinity in PDPP3T and PSBTBT could facilitate the rapid polymer reorganization and aggregation, which might lead to larger domain size and poor phase separation during the cast and dry process of blend films. While relatively low crystallinity of polymers like PBDTTT-EFT might lead to favorable morphological features with appropriate domain size and phase separation in the polymer/SDIPBI films, which can improve the charge dissociation and thereby high photocurrent. The preliminary conjecture need to be further verified by the morphological characterizations.

Successively, the surface morphology of the polymer/SDIPBI blends was investigated by atomic force microscopy (AFM) in tapping mode, as shown in Fig. 4a–h. The root-mean-square roughness (R_q) could be directly determined from the AFM height images. Thus, the R_q values were 3.31, 1.70, 5.95, and 4.20 nm for the blend films based on PBDTTPD/SDIPBI, PBDTTT-EFT/SDIPBI, PSBTBT/SDIPBI and PDPP3T/SDIPBI, respectively. It should be noted that the R_q values in PBDTTT-EFT/SDIPBI and PBDTTPD/SDIPBI systems are below 4 nm, which are consistent with the results

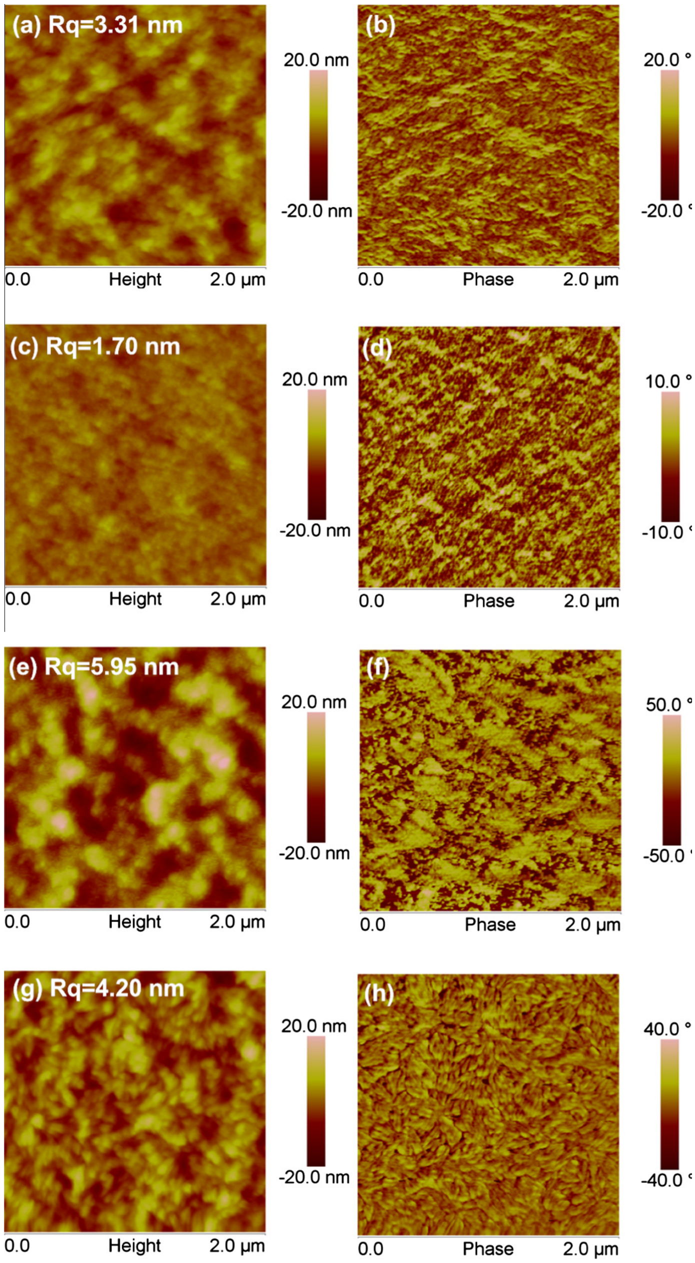

Fig. 4. AFM height and phase images of NF-PSCs based on PBDTTPD/SDIPBI (a and b), PBDTTT-EFT/SDIPBI (c and d), PSBTBT/SDIPBI (e and f) and PDPP3T/SDIPBI (g and h).

in the cases of previously reported efficient polymer/SDIPBI blends, like PBDTTT-C-T/SDIPBI [46] or PBDTBDD/SDIPBI [47] blend. In addition, PBDTTT-EFT/SDIPBI film (Fig. 4d) exhibited pronounced and interpenetrating domain feature with a moderate size of ~40 nm. Since the relatively smooth surface and small domain size facilitates the charge separation and charge collection, the excellent photovoltaic characteristic can be expected in PBDTTT-EFT/SDIPBI blend film. As shown in the phase observation in Fig. 4b, PBDTTPD/SDIPBI blend film depicts a bimodal domain feature with hundreds and tens of nanometers in length, resulting in a modest current and efficiency. On the contrary, severe phase separation and big segregated islands are observed in the PSBTBT/SDIPBI (Fig. 4f) and PDPP3T/SDIPBI blend films (Fig. 4h) as a result of higher crystallinity of PDPP3T and PSBTBT. As a result, the poor nano-scale morphology in the PSBTBT/SDIPBI and PDPP3T/SDIPBI systems generate adverse effects on the exciton dissociation and therefore drastic reduction of J_{sc} is observed (Table 2).

To obtain more information on the polymer/SDIPBI two-phased structures, we also measured the bulk morphologies of different polymer/SDIPBI blends by transmission electron microscopy (TEM) in bright field mode, as shown in Fig. 5. The PBDTTPD/SDIPBI blend film depicts some fibril-like domains and bicontinuous networks (Fig. 5a). Very different morphologies are indeed observed for PDPP3T/SDIPBI and PBDTTT-EFT/SDIPBI blend films. A rather homogeneous morphology with well-distributed domains with a feature size of ~50 nm in the PBDTTT-EFT/SDIPBI blend (see Fig. 5b). In comparison with the PBDTTT-EFT/SDIPBI blend film, the PSBTBT/SDIPBI (Fig. 5c) and PDPP3T/SDIPBI (Fig. 5d) blend films show bigger aggregations and several isolated clusters with a larger feature size of 100–200 nm, which can generate adverse effect for the charge generation and separation process [2]. The morphology of the polymer/SDIPBI blends is consistent with the values of the J_{sc} listed in Table 2. Indeed, the very low J_{sc} in PDPP3T-based NF-PSC can be clearly attributed to the declined D/A interfaces, because of the high degree of phase segregation. As referred by several reports [36,39], the photoinduced electron transfer efficiency in the low band gap polymer/PBI acceptor blends is inferior than that of the polymer/fullerene blends. This might be an intrinsic issue need to be understood and addressed with molecular engineering.

According to the XRD, AFM and TEM characterizations, we have revealed that the selection of the donor polymers is an important issue to obtain the favorable nano-scale morphology in NF-PSCs. The differences in photovoltaic performances especially current densities can be attributed to the morphological differences. Among all of the polymer/SDIPBI blend films, PBDTTT-EFT/SDIPBI film shows relatively weak π–π and lamellar stacking reflections, which could slow down the polymer crystallization and generate well-distributed domain features during film formation. This appropriate degree of crystallinity contributes to the finer nano-morphology and thus excellent device performance in PBDTTT-EFT/SDIPBI-based PSCs. In attempt to refine the selection rules of donor polymers, we find that broad absorption, appropriate energy level and optimal phase separation collectively contributed to high J_{sc} and thus good *PCE*. In addition, phase separation should be the most important factor affect the overall performance of NF-PSCs. Although PDPP3T exhibits broad absorption and appropriate energy levels, the poor phase separation severely limit the efficiency of PDPP3T/SDIPBI system. Overall, rational donor polymer selecting could be a necessary and feasible strategy to realizing high efficiency in NF-PSCs.

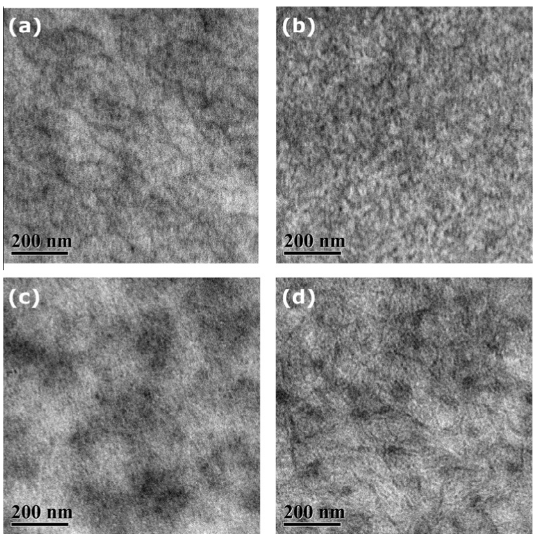

Fig. 5. TEM images of NF-PSCs based on (a) PBDTTPD/SDIPBI, (b) PBDTTT-EFT/SDIPBI, (c) PSBTBT/SDIPBI and (d) PDPP3T/SDIPBI.

4. Conclusions

To conclude, the motivation of this study is to reveal the effect of donor polymers on the microstructure, morphology, and photovoltaic performance of a specific non-fullerene acceptor and highlight the importance of donor selection in characterizing novel fullerene-free materials. Herein, detailed structure–morphology–property investigations covering absorption spectra, energy levels, crystallinity, nanoscale morphology and solar cell performances of photoactive blends of SDIPBI combined with a series of efficient low band gap donor polymers including PBDTTPD, PBDTTT-EFT, PSBTBT, PDPP3T are systematically performed. The choice of donor polymer could induce subtle changes in molecular interaction and crystallization process of polymer/SDIPBI blends, thus affecting the morphology of the polymer/SDIPBI blend film and yielding a distinct J_{sc} and *PCE* in device. Notably, the PBDTTT-EFT/SDIPBI-based PSC realized a moderate V_{oc} of 0.77 V and a high *PCE* up to 4.5%, collectively contributed by the broad absorption, appropriate HOMO level and moderate crystallinity of PBDTTT-EFT. In contrast, PDPP3T with rather broader absorption covering UV–Vis–IR region gives a much poor performance with *PCE* below 1%, which is induced by the high crystallinity and strong aggregation of PDPP3T.

On the basis of this study, a clear criterion in selection of donor polymers has been established. For a specific non-fullerene small molecule acceptor, suitable energy level differences, finer morphology, and broad absorption ranges could be successively screened and carefully explored for donor polymers. We believe that the established criterion based on SDIPBI can offer potentially important implications for other non-fullerene acceptors, and also trigger new breakthroughs for achieving highly efficient PSCs based on fullerene-free acceptor materials.

Acknowledgments

For financial support of this research, we thank the National Natural Science Foundation of China (Nos. 91333204, 21325419, 51373181), the NSFC-DFG Joint Project TRR61, and the Chinese Academy of Sciences (Nos. XDB12030200, KJZD-EW-J01).

Appendix A. Supplementary material

Supplementary data associated with this article can be found, in the online version, at http://dx.doi.org/10.1016/j.orgel.2014.12.020.

References

[1] Y.F. Li, Molecular design of photovoltaic materials for polymer solar cells: toward suitable electronic energy levels and broad absorption, Acc. Chem. Res. 45 (2012) 723–733.
[2] W. Cai, X. Gong, Y. Cao, Polymer solar cells: recent development and possible routes for improvement in the performance, Sol. Energy Mater. Sol. Cells 94 (2010) 114–127.
[3] B.A. Collins, E. Gann, L. Guignard, X. He, C.R. McNeill, H. Ade, Molecular miscibility of polymer–fullerene blends, J. Phys. Chem. Lett. 1 (2010) 3160–3166.
[4] J. Chen, Y. Cao, Development of novel conjugated donor polymers for high-efficiency bulk-heterojunction photovoltaic devices, Acc. Chem. Res. 42 (2009) 1709–1718.
[5] Z. He, H. Wu, Y. Cao, Recent advances in polymer solar cells: realization of high device performance by incorporating water/alcohol-soluble conjugated polymers as electrode buffer layer, Adv. Mater. 26 (2014) 1006–1024.
[6] A. Facchetti, Polymer donor–polymer acceptor (all-polymer) solar cells, Mater. Today 16 (2013) 123–132.
[7] G. Yu, J. Gao, J.C. Hummelen, F. Wudl, A.J. Heeger, Polymer photovoltaic cells – enhanced efficiencies via a network of internal donor–acceptor heterojunctions, Science 270 (1995) 1789–1791.
[8] Y. Lin, X. Zhan, Non-fullerene acceptors for organic photovoltaics: an emerging horizon, Mater. Horizons 1 (2014) 470–488.
[9] A.a.F. Eftaiha, J.-P. Sun, I.G. Hill, G.C. Welch, Recent advances of non-fullerene, small molecular acceptors for solution processed bulk heterojunction solar cells, J. Mater. Chem. A 2 (2014) 1201–1213.
[10] L.T. Dou, J.B. You, J. Yang, C.C. Chen, Y.J. He, S. Murase, T. Moriarty, K. Emery, G. Li, Y. Yang, Tandem polymer solar cells featuring a spectrally matched low-bandgap polymer, Nat. Photon. 6 (2012) 180–185.
[11] Z.C. He, C.M. Zhong, S.J. Su, M. Xu, H.B. Wu, Y. Cao, Enhanced power-conversion efficiency in polymer solar cells using an inverted device structure, Nat. Photon. 6 (2012) 591–595.
[12] W. Li, A. Furlan, K.H. Hendriks, M.M. Wienk, R.A.J. Janssen, Efficient tandem and triple-junction polymer solar cells, J. Am. Chem. Soc. 135 (2013) 5529–5532.
[13] T.L. Nguyen, H. Choi, S.J. Ko, M.A. Uddin, B. Walker, S. Yum, J.E. Jeong, M.H. Yun, T.J. Shin, S. Hwang, J.Y. Kim, H.Y. Woo, Semi-crystalline photovoltaic polymers with efficiency exceeding 9% in a $\sim$300 nm thick conventional single-cell device, Energy Environ. Sci. 7 (2014) 3040–3051.
[14] J. You, L. Dou, K. Yoshimura, T. Kato, K. Ohya, T. Moriarty, K. Emery, C.-C. Chen, J. Gao, G. Li, Y. Yang, A polymer tandem solar cell with 10.6% power conversion efficiency, Nat. Commun. 4 (2013) 1446.
[15] X. Guo, N. Zhou, S.J. Lou, J. Smith, D.B. Tice, J.W. Hennek, R.P. Ortiz, J.T.L. Navarrete, S. Li, J. Strzalka, L.X. Chen, R.P.H. Chang, A. Facchetti, T.J. Marks, Polymer solar cells with enhanced fill factors, Nat. Photon. 7 (2013) 825–833.
[16] C. Cabanetos, A. El Labban, J.A. Bartelt, J.D. Douglas, W.R. Mateker, J.M.J. Frechet, M.D. McGehee, P.M. Beaujuge, Linear side chains in benzo[1,2-b:4,5-b ']dithiophene-thieno[3,4-c]pyrrole-4,6-dione polymers direct self-assembly and solar cell performance, J. Am. Chem. Soc. 135 (2013) 4656–4659.
[17] C. Liu, K. Wang, X. Hu, Y. Yang, C.-H. Hsu, W. Zhang, S. Xiao, X. Gong, Y. Cao, Molecular weight effect on the efficiency of polymer solar cells, ACS Appl. Mater. Inter. 5 (2013) 12163–12167.
[18] Z.a. Tan, S. Li, F. Wang, D. Qian, J. Lin, J. Hou, Y. Li, High performance polymer solar cells with as-prepared zirconium acetylacetonate film as cathode buffer layer, Sci. Rep. 4 (2014) 4691.
[19] S. Liu, K. Zhang, J. Lu, J. Zhang, H.-L. Yip, F. Huang, Y. Cao, High-efficiency polymer solar cells via the incorporation of an amino-functionalized conjugated metallopolymer as a cathode interlayer, J. Am. Chem. Soc. 135 (2013) 15326–15329.
[20] X. Guo, M. Zhang, W. Ma, L. Ye, S. Zhang, S. Liu, H. Ade, F. Huang, J. Hou, Enhanced photovoltaic performance by modulating surface composition in bulk heterojunction polymer solar cells based on PBDTTT-C-T/$PC_{71}BM$, Adv. Mater. 26 (2014) 4043–4049.
[21] L. Ye, S. Zhang, W. Zhao, H. Yao, J. Hou, Highly efficient 2D-conjugated benzodithiophene-based photovoltaic polymer with linear alkylthio side chain, Chem. Mater. 26 (2014) 3603–3605.
[22] L. Chen, C. Xie, Y. Chen, Optimization of the power conversion efficiency of room temperature-fabricated polymer solar cells utilizing solution processed tungsten oxide and conjugated polyelectrolyte as electrode interlayer, Adv. Funct. Mater. 24 (2014) 3986–3995.
[23] S.-H. Liao, H.-J. Jhuo, Y.-S. Cheng, S.-A. Chen, Fullerene derivative-doped zinc oxide nanofilm as the cathode of inverted polymer solar cells with low-bandgap polymer (PTB7-Th) for high performance, Adv. Mater. 25 (2013) 4766–4771.
[24] P. Liu, K. Zhang, F. Liu, Y. Jin, S. Liu, T.P. Russell, H.-L. Yip, F. Huang, Y. Cao, Effect of fluorine content in thienothiophene–benzodithiophene copolymers on the morphology and performance of polymer solar cells, Chem. Mater. 26 (2014) 3009–3017.
[25] S. Zhang, L. Ye, W. Zhao, D. Liu, H. Yao, J. Hou, Side chain selection for designing highly efficient photovoltaic polymers with 2D-conjugated structure, Macromolecules 47 (2014) 4653–4659.
[26] C.-Z. Li, C.-Y. Chang, Y. Zang, H.-X. Ju, C.-C. Chueh, P.-W. Liang, N. Cho, D.S. Ginger, A.K.Y. Jen, Suppressed charge recombination in inverted organic photovoltaics via enhanced charge extraction by using a conductive fullerene electron transport layer, Adv. Mater. 26 (2014) 6262–6267.
[27] M. Zhang, X. Guo, S. Zhang, J. Hou, Synergistic effect of fluorination on molecular energy level modulation in highly efficient photovoltaic polymers, Adv. Mater. 26 (2014) 1118–1123.
[28] X. Gong, M. Tong, F.G. Brunetti, J. Seo, Y. Sun, D. Moses, F. Wudl, A.J. Heeger, Bulk heterojunction solar cells with large open-circuit voltage: electron transfer with small donor–acceptor energy offset, Adv. Mater. 23 (2011) 2272–2277.
[29] G.Q. Ren, E. Ahmed, S.A. Jenekhe, Non-fullerene acceptor-based bulk heterojunction polymer solar cells: engineering the nanomorphology via processing additives, Adv. Energy Mater. 1 (2011) 946–953.
[30] Y. Zhou, L. Ding, K. Shi, Y.Z. Dai, N. Ai, J. Wang, J. Pei, A non-fullerene small molecule as efficient electron acceptor in organic bulk heterojunction solar cells, Adv. Mater. 24 (2012) 957–961.
[31] Y.-Q. Zheng, Y.-Z. Dai, Y. Zhou, J.-Y. Wang, J. Pei, Rational molecular engineering towards efficient non-fullerene small molecule acceptors for inverted bulk heterojunction organic solar cells, Chem. Commun. 50 (2014) 1591–1594.
[32] Y. Yang, G. Zhang, C. Yu, C. He, J. Wang, X. Chen, J. Yao, Z. Liu, D. Zhang, New conjugated molecular scaffolds based on [2,2]paracyclophane as electron acceptors for organic photovoltaic cells, Chem. Commun. 50 (2014) 9939–9942.
[33] J.T. Bloking, T. Giovenzana, A.T. Higgs, A.J. Ponec, E.T. Hoke, K. Vandewal, S. Ko, Z. Bao, A. Sellinger, M.D. McGehee, Comparing the device physics and morphology of polymer solar cells employing fullerenes and non-fullerene acceptors, Adv. Energy Mater. 4 (2014) 1301426.
[34] T.V. Pho, F.M. Toma, B.J. Tremolet de Villers, S. Wang, N.D. Treat, N.D. Eisenmenger, G.M. Su, R.C. Coffin, J.D. Douglas, J.M.J. Fréchet, G.C. Bazan, F. Wudl, M.L. Chabinyc, Decacyclene triimides: paving the road to universal non-fullerene acceptors for organic photovoltaics, Adv. Energy Mater. 4 (2014) 1301007.
[35] M. Sommer, S. Huettner, M. Thelakkat, Donor–acceptor block copolymers for photovoltaic applications, J. Mater. Chem. 20 (2010) 10788–10797.
[36] I.A. Howard, F. Laquai, P.E. Keivanidis, R.H. Friend, N.C. Greenham, Perylene tetracarboxydiimide as an electron acceptor in organic solar cells: a study of charge generation and recombination, J. Phys. Chem. C 113 (2009) 21225–21232.
[37] C.R. McNeill, N.C. Greenham, Conjugated-polymer blends for optoelectronics, Adv. Mater. 21 (2009) 3840–3850.
[38] R. Singh, E. Aluicio-Sarduy, Z. Kan, T. Ye, R.C.I. MacKenzie, P.E. Keivanidis, Fullerene-free organic solar cells with an efficiency of 3.7% based on a low-cost geometrically planar perylene diimide monomer, J. Mater. Chem. A 2 (2014) 14348–14353.
[39] D.W. Gehrig, S. Roland, I.A. Howard, V. Kamm, H. Mangold, D. Neher, F. Laquai, Efficiency-limiting processes in low-bandgap polymer: perylene diimide photovoltaic blends, J. Phys. Chem. C 118 (2014) 20077–20085.
[40] S. Rajaram, R. Shivanna, S.K. Kandappa, K.S. Narayan, Nonplanar perylene diimides as potential alternatives to fullerenes in organic solar cells, J. Phys. Chem. Lett. 3 (2012) 2405–2408.
[41] R. Shivanna, S. Shoaee, S. Dimitrov, S.K. Kandappa, S. Rajaram, J.R. Durrant, K.S. Narayan, Charge generation and transport in efficient organic bulk heterojunction solar cells with a perylene acceptor, Energy Environ. Sci. 7 (2014) 435–441.
[42] X. Zhang, Z. Lu, L. Ye, C. Zhan, J. Hou, S. Zhang, B. Jiang, Y. Zhao, J. Huang, S. Zhang, Y. Liu, Q. Shi, Y. Liu, J. Yao, A potential perylene diimide dimer-based acceptor material for highly efficient solution-processed non-fullerene organic solar cells with 4.03% efficiency, Adv. Mater. 25 (2013) 5791–5797.
[43] Y. Lin, Y. Wang, J. Wang, J. Hou, Y. Li, D. Zhu, X. Zhan, A star-shaped perylene diimide electron acceptor for high-performance organic solar cells, Adv. Mater. 26 (2014) 5137–5142.
[44] Z. Lu, B. Jiang, X. Zhang, A. Tang, L. Chen, C. Zhan, J. Yao, Perylene-diimide based non-fullerene solar cells with 4.34% efficiency

through engineering surface donor/acceptor compositions, Chem. Mater. 26 (2014) 2907–2914.

[45] W. Jiang, L. Ye, X. Li, C. Xiao, F. Tan, W. Zhao, J. Hou, Z. Wang, Bay-linked perylene bisimides as promising non-fullerene acceptors for organic solar cells, Chem. Commun. 50 (2014) 1024–1026.

[46] L. Ye, W. Jiang, W. Zhao, S. Zhang, D. Qian, Z. Wang, J. Hou, Selecting a donor polymer for realizing favorable morphology in efficient non-fullerene acceptor-based solar cells, Small 10 (2014) 4658–4663.

[47] Y. Zang, C.-Z. Li, C.-C. Chueh, S.T. Williams, W. Jiang, Z.-H. Wang, J.-S. Yu, A.K.Y. Jen, Integrated molecular, interfacial, and device engineering towards high-performance non-fullerene based organic solar cells, Adv. Mater. 26 (2014) 5708–5714.

[48] J. Warnan, A. El Labban, C. Cabanetos, E.T. Hoke, P.K. Shukla, C. Risko, J.-L. Brédas, M.D. McGehee, P.M. Beaujuge, Ring substituents mediate the morphology of PBDTTPD–PCBM bulk-heterojunction solar cells, Chem. Mater. 26 (2014) 2299–2306.

[49] J. Hou, H.-Y. Chen, S. Zhang, G. Li, Y. Yang, Synthesis, characterization, and photovoltaic properties of a low band gap polymer based on silole-containing polythiophenes and 2,1,3-benzothiadiazole, J. Am. Chem. Soc. 130 (2008) 16144–16145.

[50] K.H. Hendriks, G.H.L. Heintges, V.S. Gevaerts, M.M. Wienk, R.A.J. Janssen, High-molecular-weight regular alternating diketopyrrolopyrrole-based terpolymers for efficient organic solar cells, Angew. Chem. Int. Ed. 52 (2013) 8341–8344.

[51] L. Ye, S. Zhang, W. Ma, B. Fan, X. Guo, Y. Huang, H. Ade, J. Hou, From binary to ternary solvent: morphology fine-tuning of D/A blends in PDPP3T-based polymer solar cells, Adv. Mater. 24 (2012) 6335–6341.

[52] J.-L. Wu, F.-C. Chen, Y.-S. Hsiao, F.-C. Chien, P. Chen, C.-H. Kuo, M.H. Huang, C.-S. Hsu, Surface plasmonic effects of metallic nanoparticles on the performance of polymer bulk heterojunction solar cells, ACS Nano 5 (2011) 959–967.